 doi:10.20944/preprints201806.0110.v1

Article

Novel Insights into the Configurations of Lead(II)-Benzohydroxamic Acid Coordination Compounds in Aqueous: A Combined Experimental and Computational Study

Jianyong He[1], Haisheng Han[1], Chenyang Zhang[1,*], Dandan Yuan[2], Mengjie Tian[1], Wei Sun[1, *], Yuehua Hu[1, *]

[1] School of Minerals Processing and Bioengineering, Central South University, Changsha, Hunan 410083, China.; zhangchenyang@csu.edu.cn

[2] Institute of theoretical and computational chemistry, Nanjing University, Nanjing, Jiangsu 210023, China; yddmjm@qq.com

* Correspondence: zhangchenyang@csu.edu.cn (Chenyang Zhang); sunmenghu@csu.edu.cn (Wei Sun); hyh@csu.edu.cn (Yuehua Hu). Tel:+8673188830482

Jianyong He and Haisheng Han contribute equally to this work

Abstract: Novel collector lead(II)-benzohydroxamic acid (Pb [II]-BHA) complexes in aqueous solution were characterized by using experimental approaches, including Fourier-transform infrared spectroscopy (FTIR), powder X-ray diffraction spectroscopy (PXRD), Ultraviolet-visible (UV-Vis) spectroscopy, and electrospray ionization–mass spectrometry (ESI-MS), and first-principle density functional theory (DFT) calculations with consideration of solvation effects. The Job plot delineated that a single coordinated $Pb(BHA)^+$ should be formed first, and the binary structures of $Pb(BHA)_2$ can be formed subsequently. Moreover, the Pb(II)-BHA species aggregated with each other to form highly complicated structures. ESI-MS results validated the existence of $Pb\text{-}(BHA)_{n=1,2}$. The well-consistent infrared spectra from the DFT calculations and FTIR measurements indicated that the *cis*-amide (Za)-type BHA conformer may be dominant in the solid-state crystals of BHA. The first-principle calculations suggested that $Pb(BHA)_2$ should be the most stable structure, and the Pb atom in $Pb(BHA)^+$ will play as an active site to attack nucleophiles. These findings are meaningful to further illustrate the adsorption mechanism of Pb(II)-BHA complexes in mineral processing.

Keywords: Pb(II)-BHA; lead chemistry; metal-organic collectors; DFT calculation; surface activation

1. Introduction

Metal-organic coordination complexes have been widely used in the materials, chemistry. Recently, their promising applications in mining have attracted research attention [1-8]. For instance, lead(II)-benzohydroxamic acid (Pb [II]-BHA) complexes are effective collectors in the beneficiation of oxide minerals, including tungsten minerals, cassiterite, and rutile [9,10]. Given the excellent selectivity and good collecting ability of Pb(II)-BHA, the scheelite flotation process could be simplified remarkably without the addition of sodium silicate, overcoming the shortage of heating in the routine flotation of scheelite [9-11].The beneficiation of scheelite is currently one of the most challenging problems worldwide in the field of mineral processing. Conventionally, separating scheelite from calcium bearing minerals, such as fluorite and calcite, by using anionic collectors (especially for fatty acid) is difficult due to their highly similar properties in calcium-bearing surfaces. Fortunately, our group first introduced the Pb complexes of benzohydroxamic acid (*Pb(II)-BHA complexes*) to effectively separate scheelite from calcium-bearing gangues by properly regulating the Pb/BHA ratio and pH [9,11]. Furthermore, as displayed in

Preprints (www.preprints.org) | NOT PEER-REVIEWED | Posted: 7 June 2018 doi:10.20944/preprints201806.0110.v1

Figure 1(b), the novel flotation scheme (i in Figure 1 [a]), with Pb(II)-BHA complexes used as the collector, has shown better performance than the traditional activation flotation scheme (ii in Figure 1 [a]), which first added Pb(II) as the activator and subsequently added BHA as the collector [10,12-20]. However, the effective microstructures of Pb(II)-BHA complexes in the solution and their interaction mechanisms with oxide minerals remain unclear.

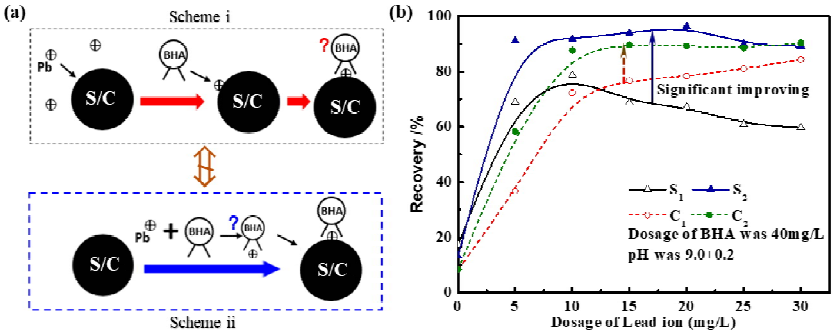

Figure 1. (a) Two flotation schemes; (b) the flotation recovery of scheelite (S) [9] and cassiterite (C) [21] as a function of dosage of Pb(II) ion (1/2 in (b) represents the flotation scheme in i and ii)..

Hydroxamic acid group (–CO–NH–OH) is the functional group of the BHA [22-24]. The functional group has relatively different properties that remain poorly characterized; in fact, a reliable assignment of the correct structure is challenging because the several possible conformations strongly depend on concentration, temperature, and the nature of the solvent [25]. The hydroxamate collectors, such as benzohydroxamic acid (BHA), naphthenic hydroxamate, and amide hydroxamate, have been well used as highly selective flotation collectors in recent years. The role to function as collectors in mineral flotation has been documented by Lynch et al. [26] However, the chelate between hydroxamic acids and metal ion has remained poorly investigated. Nowadays, first-principle calculations based on density functional theory (DFT) and some advanced experimental technologies are used to obtain more information on the molecular structure of BHA [27]. Wander et al.'s benchmarking calculations indicate that the DFT calculation can achieve near chemical accuracy of hydrolysis constants for metal ions in most cases [28]. Nuclear magnetic resonance and DFT calculations performed by Garcia et al. show that the adopted BHA conformation of BHA aqueous solution is a closed Z (cis) configuration in aqueous solution [29]. Both Z (cis) and E (trans) conformations in **Scheme 1** regularly co-existed in solvent. The concentration and environmental factors determine the ratio of Z type to E type conformations to some extent, and potential barriers are present among different conformations [30,31].

Scheme 1. BHA conformers

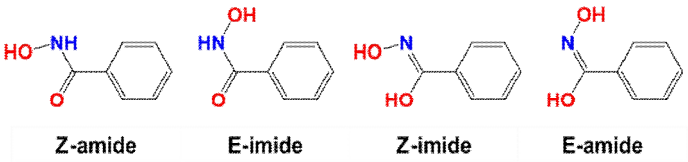

BHA can chelate with metal ions, such as copper(II) cadmium(II), cobalt(II), nickel(II), manganese(II), lead(II), zinc(II), aluminum(III), iron(III), and bismuth(III), thus taking on diverse chelate structures [23,32]. Only few heavy metal ion complexes of BHA chelates have been extensively investigated for their special uses, like the bismuth(III) complex that has activity against *Helicobacter pylori*. However, reports about the novel Pb(II)-BHA complexes are also few. Understanding of the microstructures of Pb(II)-BHA complexes is essential to improve the technique working in flotation practice and fundamental field of lead chemistry [33,34].

 doi:10.20944/preprints201806.0110.v1

This current study aims to investigate configurations of Pb(II)-BHA coordination complexes in aqueous solution. Accordingly, the powder X-ray diffraction (PXRD), Fourier-transform infrared spectroscopy (FTIR), UV-Vis spectroscopy, and electrospray ionization mass spectrometry (ESI-MS) were performed to characterize the solid and solution components. First-principle DFT calculations were performed to understand the constituents and properties of Pb(II)-BHA complexes at the molecular level. The frontier molecular orbital [35] and natural atomic orbitals (NAOs) [36] were used to describe the reactivity of the studied Pb(II)-BHA complex. This work might shed new light on effective microstructures of Pb(II)-BHA coordination complexes for mineral flotation.

2. Methodology

2.1. Experimental details

2.1.1. Materials

Analytical grade BHA and lead nitrate were purchased from Tokyo Chemical Industry Co., Ltd. in Japan. The pH value was adjusted with chemically pure sodium hydrate or hydrochloric acid stock solutions. The 18.2 MΩ pure water produced by Arium Mini Plus (Sartorius Weighing Technology, Germany) was used in this work.

2.1.2. PXRD tests

The coordination chemistry of Pb(II)-BHA is assumed to significantly change around the Pb(II)-BHA ratios of 2:1, 1:1, and 1:2. PXRD measurements on these ratios of Pb(II)-BHA were performed in transmission geometry mode in a two-theta angle range from 3° to 70°, with a step size of 0.009 using Cu $K\alpha_1$ (35 KV, 40 mA, 1.54056 Á) radiation. The patterns were collected using a diffractometer (D8 Discover, Bruker AXS, Germany) equipped with a LynxEye detector and a Johansson monochromator in the incident beam. The samples were prepared by evaporation crystallization, and all included compounds were at a concentration of 0.1 mol/L, with pure water as the solvent.

2.1.3. UV-Vis tests

The Job plot[37], proposed by Job, provides qualitative and quantitative insight into the stoichiometry with underlying association of ligand- and solvent-dependent reaction rates. The Job plot was involved to track the full reaction path. Moreover, we changed the guest and host solution to comprehensively understand the stoichiometry of the product. In this work, concentration of the Pb(II)-BHA complex, as determined by integration of the intensity of specific wavenumber, was plotted against the mole fraction X_A (the guest solution is BHA solution) and X_B (the guest solution is Pb(II) ion solution). A Shimadzu UV2600/2700 Ultraviolet spectrophotometer was used to obtain the UV-Vis spectra at a fixed concentration of Pb(II) ion at 0.1 mM by equimolar continuous change method and molar ratio method.

 doi:10.20944/preprints201806.0110.v1

2.1.4. FTIR tests

FTIR spectra between 400 and 4,000 cm^{-1} were recorded with a 740-FTIR instrument by using potassium bromide discs and reagents at a ratio of 100:1.

2.1.5. ESI-MS tests

ESI-MS spectra were collected in positive ion mode with a Bruker Q-TOF Qualification Standard Kit, using solutions of the 0.1 mM/L mixture of lead nitrate:BHA. ESI-MS spectra were used to obtain the proof of coordinated compounds of Pb(II)-BHA complexes at the molar ratio of 1:1 (at the natural pH 4.4) and 1:2 (at pH 13.0). The pH was selected according to a report that high pH can result in increased complications in solution species [10].

2.2. Computational methods

All calculations were performed with the Gaussian 09 (version D.01) quantum chemistry package, based on the B3LYP method: a three-parameter hybrid functional by replacing a certain amount of the PW91 generalized gradient approximation (GGA) correlation functional with the LYP GGA correlation functional [38-40]. Solvation effects were considered by using the polarized continuum models (PCM) in the calculation [41]. The aug-cc-pVDZ basis set was employed as all-electron basis set in all types of calculation on the light atoms H, C, N, and O, except for the Pb atom in Pb(II)-BHA complex systems. The aug-cc-pVDZ-PP basis set with a relativistic pseudopotential was used for the Pb atom. The basis set, obtained from EMSL Basis Set Exchange web site, has already been verified to produce acceptable thermodynamic information of hydrated Pb (II) ion[42-44]. The Los Alamos effective core potential double-ξ (LanL2Dz) was used for the primary geometry optimization of modelled benzohydroxamic acid and its Pb (II) complex in ionic form. LanL2Dz replaced 78 core electrons with relativistic effective core potential (RECP) [45]; therefore, only two valence electrons of Pb(II) ions were described [46]. To refine the structure and calculate the molecular orbitals, we further used the larger aug-cc-pVDZ basis set for the light atoms, such as hydrogen, oxygen, nitrogen, and carbon, and we used the aug-cc-pVDZ–PP with RECP of the inner 60 electrons for Pb(II) ions to calculate the frequency [47]. The default convergence parameters (with maximum force within 4.5×10^{-4}, force RMS within 1.8×10^{-3}) in the Gaussian 09 software were retained to optimize the structure. All calculations were successfully converged, without virtual frequencies in the vibration analysis.

In the building of BHA anion model [48], the proton at the carbonyl oxygen was removed according to the preferred deprotonation site reported by Begoña et al. and Arora et al. [29,49]. The Pb(II) ion was set as the metal center ion which would be the coordination center of the bidentate BHA anions. The envisaged conformations were ligated by two, three and four BHA anions. Thermodynamic values for Gibbs free energy [50] were obtained using the PCM with the context:

Preprints (www.preprints.org) | NOT PEER-REVIEWED | Posted: 7 June 2018 doi:10.20944/preprints201806.0110.v1

$$\Delta G_r = \sum G_{prod} - \sum G_{react} \quad (1)$$

where G_{prod} and G_{react} are the free energy or the products and the reactants included in the reaction, respectively.

Gauss View was used as a visualization tool in this paper. In addition, all calculations including the mapped molecular orbitals in this work were performed at the theory level of PCM -B3LYP/aug-cc-pVDZ on light atoms and PCM -B3LYP/aug-cc-pVDZ-PP on Pb atom [51]. Molecular orbital contours for the highest occupied molecular orbital (HOMO) and the lowest unoccupied molecular orbital (LUMO) of the cluster model were computed at the same theoretical level. The contribution of Pb atom to the frontier molecular orbitals were calculated with a multifunctional wavefunction analyzer Multiwfn [52] based on the NAOs.

3. Results and discussion

3.1. Experimental

3.1.1. PXRD results

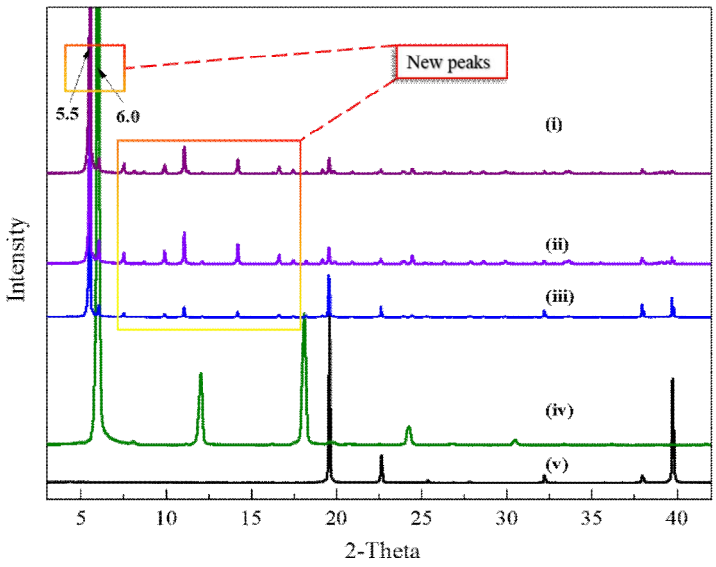

Figure 2. PXRD spectra of Pb(II)-BHA mixtures at Pb:BHA molar ratios of (i) 2:1, (ii) 1:1, and (iii) 1:2, and pure reagents of (iv) BHA and (v) lead nitrate.

Figure 2 depicts the PXRD spectra of the evaporation-crystalized samples at a series of planned molar ratios, which are described in the Methodology section. The consistently strong sharp peaks at Pb:BHA molar ratios of (i) 2:1, (ii) 1:1, and (iii) 1:2 suggest a favorable crystallinity and size homogeneity of the product, and the coordination compounds should have a well-organized

Preprints (www.preprints.org) | NOT PEER-REVIEWED | Posted: 7 June 2018 doi:10.20944/preprints201806.0110.v1

structure. We focused on the structure of Pb(II)-BHA complexes in the aqueous solution, these characteristic peaks of the raw reactants, BHA (iv) and lead nitrate (v), used for the synthesis reaction, did not influence further conclusions. The PXRD results of BHA crystal structure in our results coincided with those results from Podlaha et al., showing similar spectra of an iron-BHA crystal [53]. Pb(II)-BHA complexes may contribute to these peaks at 5.5°, 7.5°, 9.9°, 11.1°, 14.2°, and 16.6°, which were reassembled with the metal-organic frame network of metal-BHA frame system with a typical π-π stacking structure [54]. Unfortunately, our attempts to grow a single crystal of the Pb(II)-BHA complex in aqueous solution to validate this hypothesis were unsuccessful.

3.1.2. UV-Vis results

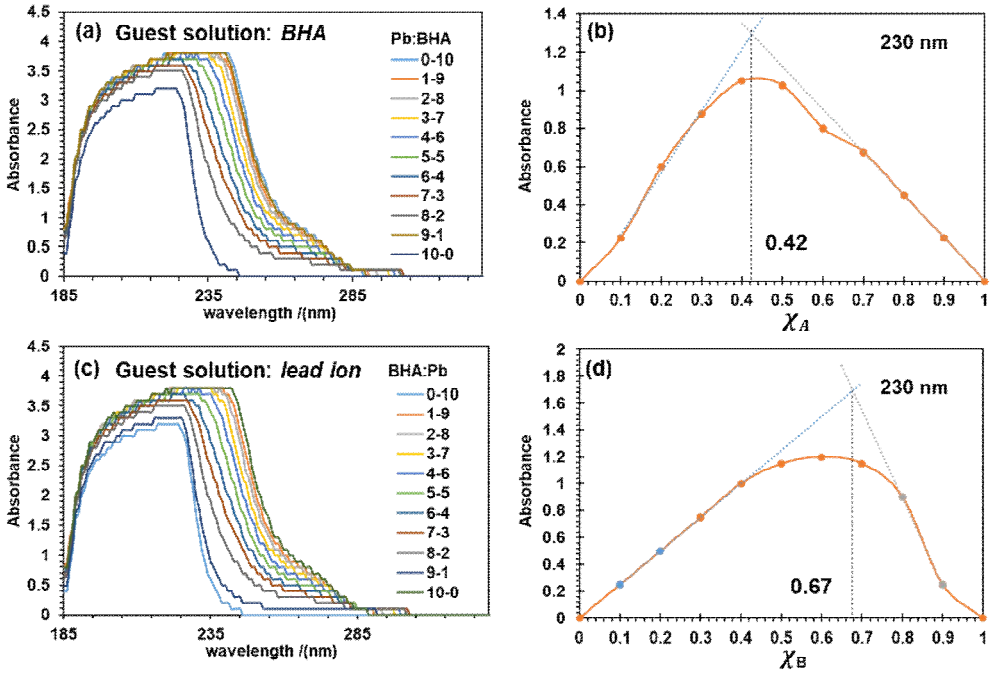

Figure 3. (a) The plotted UV-Vis absorbance spectra (c) spanning the wavelength from 185 nm to 325 nm, and (b) Job plots (d) at 230 nm for the prepared solutions with BHA (Pb [II]) as a guest solution. X_A and X_B are the mole fractions of Pb(II) ions and BHA according to dosing methods 1 and 2, respectively. All stock solutions are prepared at 1 mM/L concentration.

Because of the superposition of UV-Vis absorbance peaks of the products and the reactants, carefully processing the collected UV-Vis data is essential. Initially, the first and the last points were fixed at zero absorbance because the complexity of the product might be relatively different when one component is in excess, and the further fitting procedures would exclude the two points [55]. The start second point and the last second point were connected to form a background. After deducing the background absorption, the Job plots were plotted, as shown in **Figures 3(b)** and **3(d)**. Herein, Job plots were fitted using the method of initial tangents using experimental data close to the beginning points (the first and last points were not included due to the formation of hydrated Pb

Preprints (www.preprints.org) | NOT PEER-REVIEWED | Posted: 7 June 2018 doi:10.20944/preprints201806.0110.v1

complexes and the solvation of BHA) [56]. As illustrated in **Figure 3**, X_A and X_B were the mole fractions of Pb(II) ions and BHA according to dosing methods 1 and 2, respectively. The wavelength at 230 nm represents the significant changes in the solution components. The same trends can also be obtained by using other wavelengths between 230 and 240 nm (**Figure 4**). In addition, the order that we prepared the mixture for the UV-Vis tests can influence the reaction paths. The accepted potential reaction mechanism might be described as follows:

$$BHA^- + Pb^{2+} \rightarrow Pb(BHA)^+ \overset{BHA^-}{\rightarrow} Pb(BHA)_2 \quad (2)$$

$$2BHA^- + Pb^{2+} \rightarrow Pb(BHA)_2 \quad (3)$$

where **Equation (2)** could be explained as the stepwise formation of the single coordinated $Pb(BHA)^+$ complex, when a small quantity of BHA^- solution was used as a guest species, and Equation (3) is ideal for interpreting the formation of $Pb(BHA)_2$, when Pb(II) solution was used as a guest species.

Figures 3(a) and **3(c)** show that the increasing dosage of Pb(II) ions and BHA strengthened and extended the absorbance peaks. Job plots were obtained from newly mixed Pb(II)-BHA mixture, with the collected characteristic absorbance peaks of UV-Vis spectra in aqueous solution having both dosing methods. The absorbance peak at 230 nm was plotted with respect to the range of the molar ratios of Pb(II):BHA from 1:9 to 9:1. The obtained Job plots showed that the stoichiometry of the complexes for the first one with BHA as a guest solution was X_A = 0.42 (**Figure 3 [b]**), which supported a stoichiometry of Pb(II):BHA between 1:1 to 1:2. Meanwhile, the reversing dosing method with Pb(II) ion solution as guest solution obtained X_B = 0.67 (**Figure 3 [d]**), clearly indicating that a stoichiometry of 1:2 corresponded to the structure of $Pb(BHA)_2$. These results supported the formation of $Pb(BHA)_2$ complex when excessive BHA solution was added.

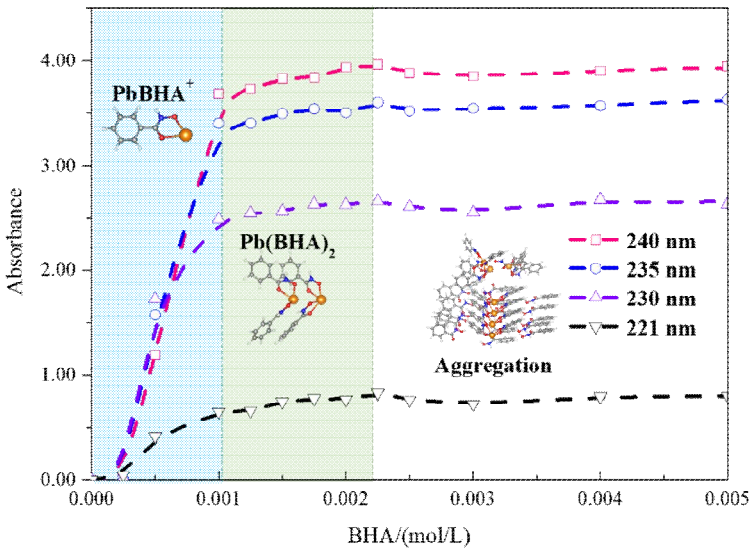

Preprints (www.preprints.org) | NOT PEER-REVIEWED | Posted: 7 June 2018 doi:10.20944/preprints201806.0110.v1

Figure 4. UV-Vis absorbance changes of 1 mM/L Pb(II) ion solution with respect to the continuous addition of BHA (at wavelengths of 221, 230, 235, and 240 nm), based on the continuous concentration change method. Spheres for atoms Pb, C, H, O, and N in the inset are colored in orange, grey, white, red, and blue, respectively.

Figure 4 shows the further UV-Vis test results at the characteristic peaks of 221, 230, 235, and 240 nm that could explain the mechanism of forming high coordination complexes. These drawn curves showed a consistent trend. For a clear illustration, we divided these curves into three stages. At the beginning stage, the absorbance increased rapidly. At the end of the rising stage at 1 mM/L of BHA, a 1:1 Pb(II)-BHA complex was formed, which was consistent with both the obtained result of the $Pb(BHA)^+$ complex in the Job plots and the computational section. Afterward, the curves showed a slow rising stage region with a small slope from 1 nM/L to 2.5 mM/L. The fluctuation of these collected data suggested that the component in the solution should be intricate. Interestingly, these trends ended with the same proportion of Pb:BHA = 1:2.5, at which the $Pb(BHA)_2$ complex might existed as indicated by the Job plots. When increasing the BHA concentration, these curves adopted a horizontal line-like region of the similar absorbance intensity to pure BHA solution. The three stages in the curve can be seen as the stepwise formation of high coordination complexes, as interpreted by **Equation (2)**.

3.1.3. ESI-MS spectra

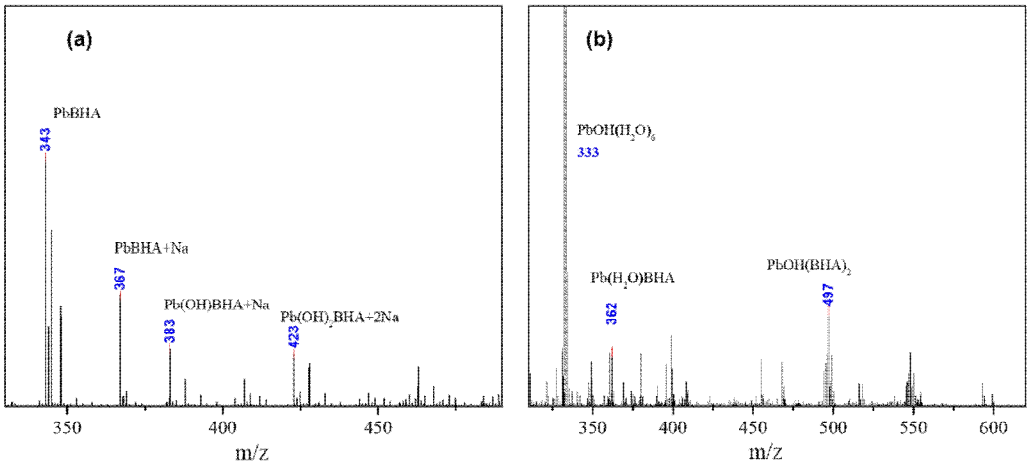

Figure 5. ESI-MS spectra of the mixture of (a) Pb:BHA molar ratio of 1:1 at a pH value of 13.0 and (b) Pb:BHA molar ratio of 1:2 at the natural pH of 4.4. (Solution concentrations are 1 mM/L.)

To identify possible Pb(II)-BHA complexes formed in the solution, the collected ESI-MS data of reaction mixtures of lead nitrate and BHA with water as solvent are shown in **Figure 5**. **Figure 5(a)** shows that when the solution pH is approximately 13.0 in the mixture, the main product is the single coordination complex. **5(b)** shows that Pb(II)-BHA complex at the molar ratio of 1:2 can produce single and double coordination products in aqueous solution. The direct proof of the single coordinated Pb(II) complex and double coordinated complex with BHA as ligands was provided, indicating that the $Pb(BHA)^+$, $Pb(BHA)_2$, and the possible high coordination complex were formed in

Preprints (www.preprints.org) | NOT PEER-REVIEWED | Posted: 7 June 2018 doi:10.20944/preprints201806.0110.v1

a stepwise order. This finding was consistent with the result obtained from the continuous concentration change method. Meanwhile, the findings of the hydrated Pb(II) of $PbOH(H_2O)_6$ and the Pb(II)-BHA complex, as shown in **Figure 5(b),** suggested that the hydration shell of Pb(II) might be dissociated due to the coordination reaction.

The ESI-MS result validated the existence of the Pb(II) complex with one and two BHA as ligands. The experimental approaches were not sufficient to provide exact structures or properties; thus, the structure of Pb(II)-BHA complexes, considering the solvation effects, were further studied using first-principle DFT calculations at high accuracy.

3.2. Theoretical prediction results

3.2.1. Prediction of stable BHA isomers and Pb(II)-BHA complexes

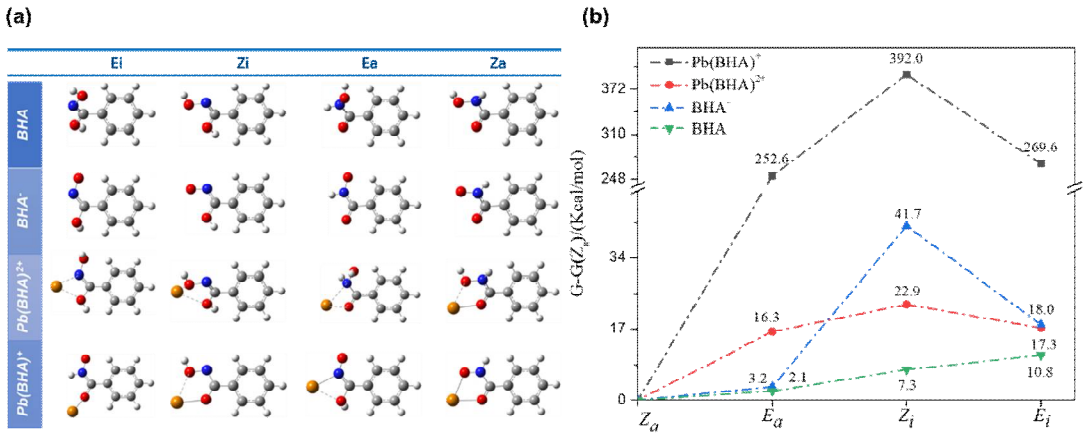

Figure 6. (a) Optimal structures of BHA, BHA^-, $Pb(BHA)^{2+}$, and $Pb(BHA)^+$. (b) Comparison of Gibbs free energy of the single coordinated Pb ion with BHA and BHA anion as ligand with the Gibbs free energy of Za type as a zero level. Spheres for Pb, C, H, O, and N atoms are colored in orange, grey, white, red, and blue.

All optimized BHA and BHA^- (the anion of the BHA molecule with the dissociation of the proton) structures are shown in the first two rows in **Figure 6(a)** at a B3LYP/aug-cc-pVDZ theoretical level. Notably, the molecules are not a plane because of the existence of the conjugated effect (the Cartesian coordinate file of these structures are available from the corresponding authors). The optimal structures are marked with Z and E types. From the calculation results, a stable five membered ring binds with the so called O-O' of Za type anion [23].

Phenyl is an electron-withdrawing group in the BHA having the structure of an electron donor; thus, the hydroxamic group in Za type as a bi-dentate ligand can chelate with Pb(II) ligands. The optimal Za-type BHA possesses the lowest ground state of Gibbs free energy, indicating that the Za-type BHA should be the most stable structure. **Figure 6(b)** shows that the supported configurations (according to the calculated Gibbs free energies) of the Pb(II)-BHA complexes are the

Preprints (www.preprints.org) | NOT PEER-REVIEWED | Posted: 7 June 2018 doi:10.20944/preprints201806.0110.v1

coordination compounds of Pb(II)-Za-type structures. The Gibbs free energy between the Za and Zi isomers shows a small difference, implying that the transformation between isomers might exist. According to Arora et al. [49], the energy barriers among these BHA isomers are small and can be overcome. The existence of transformations among different isomers suggests that FTIR tests might be difficult to obtain a fully matched spectrum with calculation results due to the vibrational coupling.

3.2.2. Experimental and Computational Vibrational Spectra

Vibrational spectrums by theoretical calculations and the experimental spectrums are shown in **Figure 7**. The obtained correction of **Equation (4)** by Arora et al. [49], with the regression analysis method, was used to correct the shift in the calculation results. The IR vibration spectra of the BHA isomers are obtained from the frequency calculation, stated as follows:

$$\tilde{\nu} = 0.939\tilde{\nu}_{calc} + 48.9(r = 0.999) \quad (4)$$

where $\tilde{\nu}_{calc}$ is the calculated wavelength, and $\tilde{\nu}$ is the corrected wavelength. A comparative study of the experimental vibration spectra of BHA solid and the cluster models are plotted in **Figure 7**.

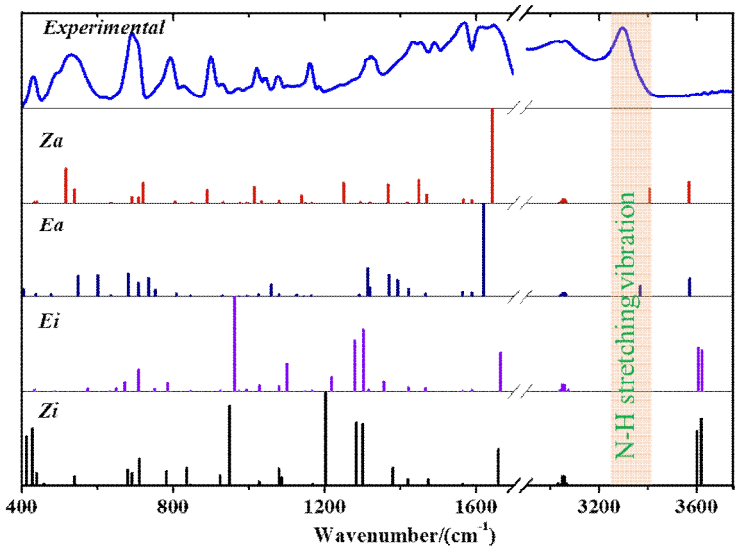

Figure 7. Theoretical calculation of BHA isomers and experimental infrared (IR) results of BHA solid (calculations at the theory level of PCM-B3LYP/aug-cc-pVDZ).

Figure 7 shows the middle IR spectra (wavenumber ranges from 400–4,000 cm^{-1}) of the pure BHA and the calculated vibrational spectrums of these isomers. The top spectrum is the experimental FTIR spectrum, where the strong characteristic peak at 3,295 cm^{-1} can be assigned as

Preprints (www.preprints.org) | NOT PEER-REVIEWED | Posted: 7 June 2018 doi:10.20944/preprints201806.0110.v1

the N–H stretching vibration coupling with the O–H stretching vibration, corresponding to the calculation results of Za at 3,468 cm^{-1} and Ea at 3,405 cm^{-1}. No characteristic peaks of hydroxyl in the sample were noted, implying that the imide-type isomers are certainly few. The comparison of theoretical and experimental IR spectra shows that the coupling of the characteristic absorption peaks may exist. The experimental IR results and the calculated spectra suggest that the amide types of BHA may dominate the solid-state BHA.

3.2.3. High coordination complexes

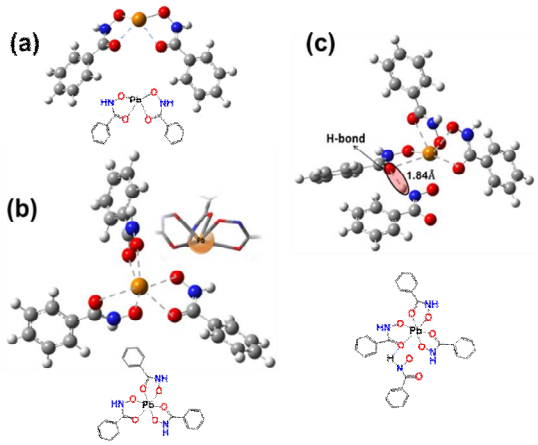

Figure 8. Optimal structures of Pb(II)-BHA with coordination numbers (CN) of 2 (a), 3 (b), and 4 (c). Spheres for Pb, C, H, O, and N atoms are colored in orange, grey, white, red, and blue.

Table 1. The changes in Gibbs free energy (ΔGr) and Pb–O mean distance in Pb(II)-BHA complexes with CN of BHA ligands ranging from 1 to 3.

CN	Reaction	ΔGr(Kcal/mol)	Pb-O ( )	ε_{gap} (eV)
1	Pb^{2+}+BHA^{-}	-356.55	2.26	4.17
2	$Pb(BHA)^{+}$+BHA^{-}	-27.20	2.40	4.50
3	$Pb(BHA)_2$+BHA^{-}	+0.03	2.58	4.17

In thermodynamics, the isomer having the lowest Gibbs free energy (**G**) can be the most stable and efficient isomer; Za-type structures should be the stable configurations and the dominant components according to the Gibbs free energies shown in **Figure 6(b)**, which is consistent with the obtained result by Begoña et al. [29]. The Za-type structure as the ligand has been used for the subsequent calculations. The initial Pb(II)-BHA coordination complexes are modeled based on the Pb(II) ion as the central metal ion, based on the stepwise mechanism in **Equation 2**. To obtain the possible high coordination compounds, we increased the number of BHA ligand to 4.

Preprints (www.preprints.org) | NOT PEER-REVIEWED | Posted: 7 June 2018 doi:10.20944/preprints201806.0110.v1

As shown in **Figure 8**, all Pb(II)-BHA coordination complexes adopt hemidirected geometry; in such configuration, BHA ligands occupy merely half of the space surrounding the Pb(II) atom [7,46,57]. As shown in **Table 1**, the first BHA chelated with Pb(II) corresponds to a total reaction free energy change of -356.55 Kcal/mol, indicating a strong binding interaction. For the second BHA^- ligand, a total reaction free energy change is -27.20 Kcal/mol, excluding the formation free energy of $Pb(BHA)^+$. Thereafter, the third BHA^- results in a positive change in Gibbs free energy of 0.03 Kcal/mol, implying that the binding of the third one with the former $Pb(BHA)_2$ is inefficient in thermodynamics. Moreover, when CN reaches 4, the intramolecular aggregation occurred by a hydrogen bonding interaction between the added BHA^- and another adjoining BHA^-. As shown in **Figure 8(c)**, the intermolecular distance between the H–O is 1.84 Á, indicating that the CN higher than 3 results in aggregation of adjoining BHA [23,58]. Because the calculation for this system was costly and may not produce helpful results, we did not perform the frequency calculation for this Pb(II) complex with four BHAs as ligands. In all, in an experimental test, the complexes with two BHA ligands may be ultimately measured. A higher CN than 3 might not be stable, but a Pb(II)-BHA complex with 3 or more BHA ligands may appear due to the intermolecular interactions, including the Van der Waals' force, H-bonding interaction, and the π-π stacking of benzene rings. This finding agrees with the PXRD results with a π-π stacking structure.

3.2.4. Frontier molecular orbital analysis

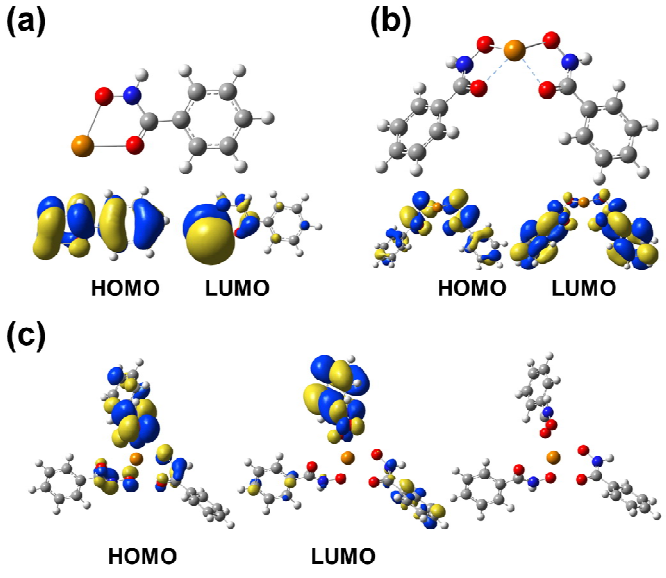

Figure 9. The frontier molecular orbitals (HOMO and LUMO) of Pb(II)-BHA complexes with 1 (a), 2 (b), and 3 (c) BHA ligands. The orbitals are calculated at the B3LYP theory level with a threshold of 0.001 au, and the solvation effect is included with PCM model. Spheres for Pb, C, H, O, and N atoms are colored in orange, grey, white, red, and blue.

Preprints (www.preprints.org) | NOT PEER-REVIEWED | Posted: 7 June 2018 doi:10.20944/preprints201806.0110.v1

Table 2. The contribution of the Pb atom to frontier molecular orbitals (HOMO+1, HOMO, LUMO, and LUMO-1) based on the NAO[59] method

Pb-BHA	Orbital composition assigned to Pb atom/%			
	HOMO-1	HOMO	LUMO	LUMO+1
$Pb(BHA)^+$	0.03	3.55	91.93	77.54
$Pb(BHA)_2$	1.14	1.28	1.14	0.02
$Pb(BHA)_3^-$	1.01	0.75	0.13	0.00

In Figure 9, the ligands of $Pb(BHA)_2$ (b) and[$Pb(BHA)_3$ (c) occupied merely one half of the space surrounding the Pb(II) ions. $Pb(BHA)_2$ and $Pb(BHA)_3^-$ adopted the hemidirected Pb(II)–BHA structures due to the lone pair electron contributed by BHA ligands [46,60]. Additionally, the structure of BHA can form some dimer structures and even interplay with themselves. The adjoining BHA may result in aggregation due to intermolecular interaction [29].

4. Conclusions

In the present study, we investigated the Pb(II)-BHA complexes though experimental and computational approaches, and the solvation effects were considered. The accepted stable Pb(II)-BHA complex structures are $Pb(BHA)^+$ and $Pb(BHA)_2$.

PXRD spectra show that the structures of the product of the Pb-BHA mixture should be well-organized. Job plots of two dosing methods indicate that the Pb coordination compounds in solution may adopt stoichiometry of $Pb(BHA)^+$ and $Pb(BHA)_2$. UV-Vis results by equimolar continuous change method show that the $Pb(BHA)^+$ and $Pb(BHA)_2$ compounds should be formed stepwise in aqueous solution. Furthermore, ESI-MS spectra provide the direct proof of the $Pb(BHA)^+$ and $Pb(BHA)_2$ in aqueous solution. The first-principle DFT calculations show that the Za-type BHA structure may dominate in the BHA solution. Further optimized $Pb(BHA)^+$ and $Pb(BHA)_2$ are the adopted structures by thermodynamics, and highly coordinated Pb(II)-BHA complex is inefficient in thermodynamics. The Pb atom contributes mainly to the LUMO, suggesting that the Pb atom in the structure should be the active site to accept nucleophile. These findings are meaningful to further illustrate the adsorption mechanism of Pb(II)-BHA complexes in mineral processing.

Acknowledgments: The work was supported by the Found of State Key Laboratory of Mineral Processing (No. BGRIMM-KJSKL-2017-13); Natural Science Foundation of China (No. 51704330;51374247); the Startup Fund of Central South University for Young Teachers (502044001); the National 111 Project (No. B14034); Collaborative Innovation Center for Clean and Efficient utilization of Strategic Metal Mineral Resources; Innovation Driven Plan of Central South University (No. 2015CX005); The Innovation Program for Postgraduate Students of Central South University (No. 502211846) and the National Science and Technology Support Project of China. This work was carried out in part using hardware and/or software provided by a Tianhe II supercomputer at the National Supercomputing Center in Guangzhou, and the High-Performance Computing Centers of Central

South University and Nanjing University. ESI-MS measurements were conducted at the Modern Analysis and Testing Center of CSU.

References

1. Hou, G.L.; Chen, B.; Transue, W.J.; Yang, Z.; Grutzmacher, H.; Driess, M.; Cummins, C.C.; Borden, W.T.; Wang, X.B. Spectroscopic characterization, computational investigation, and comparisons of ecx- (e = as, p, and n; x = s and o) anions. *J Am Chem Soc* **2017**, *139*, 8922-8930.
2. Kuta, J.; Clark, A.E. Trends in aqueous hydration across the 4f period assessed by reliable computational methods. *Inorg Chem* **2010**, *49*, 7808-7817.
3. Aguilo, E.; Moro, A.J.; Gavara, R.; Alfonso, I.; Perez, Y.; Zaccaria, F.; Guerra, C.F.; Malfois, M.; Baucells, C.; Ferrer, M.*, et al.* Reversible self-assembly of water-soluble gold(i) complexes. *Inorg Chem* **2017**.
4. Akturk, E.S.; Scappaticci, S.J.; Seals, R.N.; Marshak, M.P. Bulky beta-diketones enabling new lewis acidic ligand platforms. *Inorg Chem* **2017**, *56*, 11466-11469.
5. Bhatta, S.R.; Mondal, B.; Vijaykumar, G.; Thakur, A. Ict-isomerization-induced turn-on fluorescence probe with a large emission shift for mercury ion: Application in combinational molecular logic. *Inorg Chem* **2017**, *56*, 11577-11590.
6. Choi, K.M.; Kim, D.; Rungtaweevoranit, B.; Trickett, C.A.; Barmanbek, J.T.; Alshammari, A.S.; Yang, P.; Yaghi, O.M. Plasmon-enhanced photocatalytic co(2) conversion within metal-organic frameworks under visible light. *J Am Chem Soc* **2017**, *139*, 356-362.
7. Jalilehvand, F.; Sisombath, N.S.; Schell, A.C.; Facey, G.A. Lead(ii) complex formation with l-cysteine in aqueous solution. *Inorg Chem* **2015**, *54*, 2160-2170.
8. Li, J.; Yu, X.; Xu, M.; Liu, W.; Sandraz, E.; Lan, H.; Wang, J.; Cohen, S.M. Metal-organic frameworks as micromotors with tunable engines and brakes. *J Am Chem Soc* **2017**, *139*, 611-614.
9. Han, H.; Hu, Y.; Sun, W.; Li, X.; Chen, K.; Zhu, Y.; Nguyen, A.V.; Tian, M.; Wang, L.; Yue, T.*, et al.* Novel catalysis mechanisms of benzohydroxamic acid adsorption by lead ions and changes in the surface of scheelite particles. *Minerals Engineering* **2018**, *119*, 11-22.
10. Tian, M.; Hu, Y.; Sun, W.; Liu, R. Study on the mechanism and application of a novel collector-complexes in cassiterite flotation. *Colloids and Surfaces A: Physicochemical and Engineering Aspects* **2017**, *522*, 635-641.
11. Han, H.; Hu, Y.; Sun, W.; Li, X.; Cao, C.; Liu, R.; Yue, T.; Meng, X.; Guo, Y.; Wang, J.*, et al.* Fatty acid flotation versus bha flotation of tungsten minerals and their performance in flotation practice. *Int. J. Miner. Process.* **2017**, *159*, 22-29.
12. Sun, L.; Hu, Y.-h.; Sun, W. Effect and mechanism of octanol in cassiterite flotation using benzohydroxamic acid as collector. *Transactions of Nonferrous Metals Society of China* **2016**, *26*, 3253-3257.
13. Gao, Z.Y.; Sun, W.; Hu, Y.H. New insights into the dodecylamine adsorption on scheelite and calcite: An adsorption model. *Minerals Engineering* **2015**, *79*, 54-61.
14. Han, H.-S.; Liu, W.-L.; Hu, Y.-H.; Sun, W.; Li, X.-D. A novel flotation scheme: Selective flotation of tungsten minerals from calcium minerals using pb–bha complexes in shizhuyuan. *Rare Metals* **2017**, *36*, 533-540.
15. Hu, Y.; Qiu, G.; Miller, J.D. Hydrodynamic interactions between particles in aggregation and flotation. *Int. J. Miner. Process.* **2003**, *70*, 157-170.
16. Zhao, G.; Wang, S.; Zhong, H. Study on the activation of scheelite and wolframite by lead nitrate. *Minerals* **2015**, *5*, 247-258.

17. Filippova, I.V.; Filippov, L.O.; Duverger, A.; Severov, V.V. Synergetic effect of a mixture of anionic and nonionic reagents: Ca mineral contrast separation by flotation at neutral ph. *Minerals Engineering* **2014**, *66-68*, 135-144.
18. Deng, L.; Zhao, G.; Zhong, H.; Wang, S.; Liu, G. Investigation on the selectivity of n-((hydroxyamino)-alkyl) alkylamide surfactants for scheelite/calcite flotation separation. *Journal of Industrial and Engineering Chemistry* **2016**, *33*, 131-141.
19. Chen, Z.; Ren, Z.; Gao, H.; Lu, J.; Jin, J.; Min, F. The effects of calcium ions on the flotation of sillimanite using dodecylammonium chloride. *Minerals* **2017**, *7*, 28.
20. Materna, K.L.; Crabtree, R.H.; Brudvig, G.W. Anchoring groups for photocatalytic water oxidation on metal oxide surfaces. *Chemical Society reviews* **2017**, *46*, 6099-6110.
21. Tian, M.; Gao, Z.; Han, H.; Sun, W.; Hu, Y. Improved flotation separation of cassiterite from calcite using a mixture of lead (ii) ion/benzohydroxamic acid as collector and carboxymethyl cellulose as depressant. *Minerals Engineering* **2017**, *113*, 68-70.
22. Schraml, J. Derivatives of hydroxamic acids. *Applied Organometallic Chemistry* **2000**, *14*, 604-610.
23. Codd, R. Traversing the coordination chemistry and chemical biology of hydroxamic acids. *Coordination Chemistry Reviews* **2008**, *252*, 1387-1408.
24. Flipo, M.; Charton, J.; Hocine, A.; Dassonneville, S.; Deprez, B.; Deprez-Poulain, R. Hydroxamates: Relationships between structure and plasma stability. *Journal of medicinal chemistry* **2009**, *52*, 6790-6802.
25. Al-Saadi, A.A. Conformational analysis and vibrational assignments of benzohydroxamic acid and benzohydrazide. *Journal of Molecular Structure* **2012**, *1023*, 115-122.
26. Lynch, A.J.; Watt, J.S.; Fich, J.A.; Harbort, G.J. History of flotation technology. **2007**, 65-91.
27. Lei, X.L.; Pan, B.C. The geometries and proton transfer of hydrated divalent lead ion clusters [pb(h2o)n]2+(n = 1–17). *Journal of Theoretical & Computational Chemistry* **2012**, *11*, 1149-1164.
28. Wander, M.C.; Rustad, J.R.; Casey, W.H. Influence of explicit hydration waters in calculating the hydrolysis constants for geochemically relevant metals. *Journal of Physical Chemistry A* **2010**, *114*, 1917.
29. García, B.; Ibeas, S.; Leal, J.M.; Secco, F.; Venturini, M.; Senent, M.L.; Niño, A.; Muñoz, C. Conformations, protonation sites, and metal complexation of benzohydroxamic acid. A theoretical and experimental study. *Inorganic Chemistry* **2005**, *44*, 2908.
30. Adiguzel, E.; Yilmaz, F.; Emirik, M.; Ozil, M. Synthesis and characterization of two new hydroxamic acids derivatives and their metal complexes. An investigation on the keto/enol, e/z and hydroxamate/hydroximate forms. *Journal of Molecular Structure* **2017**, *1127*, 403-412.
31. Caudle, M.T.; Crumbliss, A.L. Dissociation kinetics of (n-methylacetohydroxamato)iron(iii) complexes: A model for probing electronic and structural effects in the dissociation of siderophore complexes. *Computational Optimization & Applications* **2009**, *43*, 353-377.
32. O'Brien, E.C.; Farkas, E.; Gil, M.J.; Fitzgerald, D.; Castineras, A.; Nolan, K.B. Metal complexes of salicylhydroxamic acid (h2sha), anthranilic hydroxamic acid and benzohydroxamic acid. Crystal and molecular structure of [cu(phen)2(cl)]cl x h2sha, a model for a peroxidase-inhibitor complex. *Journal of Inorganic Biochemistry* **2000**, *79*, 47-51.
33. Bodwin, J.J.; Cutland, A.D.; Malkani, R.G.; Pecoraro, V.L. Cheminform abstract: The development of chiral metallacrowns into anion recognition agents and porous materials. *Coordination Chemistry Reviews* **2001**, *s 216–217*, 489-512.
34. Pereira, C.F.; Howarth, A.J.; Vermeulen, N.A.; Almeida Paz, F.A.; Tomé, J.P.C.; Hupp, J.T.; Farha, O.K. Towards hydroxamic acid linked zirconium metal–organic frameworks. *Mater. Chem. Front.* **2017**, *1*, 1194-1199.

 doi:10.20944/preprints201806.0110.v1

35. Fukui, K.; Yonezawa, T.; Nagata, C. Theory of substitution in conjugated molecules. *Bull.chem.soc.jpn* **1954**, *27*, 423-427.
36. Glendening, E.D.; Landis, C.R.; Weinhold, F. Natural bond orbital methods. *Wiley Interdisciplinary Reviews: Computational Molecular Science* **2012**, *2*, 1-42.
37. Renny, J.S.; Tomasevich, L.L.; Tallmadge, E.H.; Collum, D.B. Method of continuous variations: Applications of job plots to the study of molecular associations in organometallic chemistry. *Angewandte Chemie* **2013**, *52*, 11998-12013.
38. Frisch, M.; Trucks, G.; Schlegel, H.B.; Scuseria, G.; Robb, M.; Cheeseman, J.; Scalmani, G.; Barone, V.; Mennucci, B.; Petersson, G. Gaussian 09, revision d. 01. Gaussian, Inc., Wallingford CT: 2009.
39. Becke, A.D. Becke's three parameter hybrid method using the lyp correlation functional. *J. Chem. Phys* **1993**, *98*, 5648-5652.
40. Yu, H.S.; Li, S.L.; Truhlar, D.G. Perspective: Kohn-sham density functional theory descending a staircase. *J Chem Phys* **2016**, *145*, 130901.
41. Ho, J.; Ertem, M.Z. Calculating free energy changes in continuum solvation models. *The journal of physical chemistry. B* **2016**, *120*, 1319-1329.
42. Feller, D. The role of databases in support of computational chemistry calculations. *Journal of Computational Chemistry* **1996**, *17*, 1571-1586.
43. Malekghassemi, M. An exploration of molecular mechanics and quantum chemical methods.
44. Lei, X.L.; Pan, B.C. The geometries and proton transfer of hydrated divalent lead ion clusters [pb(h2o)n]2+(n = 1–17). *Journal of Theoretical and Computational Chemistry* **2012**, *11*, 1149-1164.
45. Lee, Y.S.; Ermler, W.C.; Pitzer, K.S. Ab initio effective core potentials including relativistic effects. V. Scf calculations with ω–ω coupling including results for au2+, tlh, pbs, and pbse. *The Journal of Chemical Physics* **1980**, *73*, 360-366.
46. Wander, M.C.F.; Clark, A.E. Hydration properties of aqueous pb(ii) ion. *Inorganic Chemistry* **2008**, *47*, 8233.
47. Ochterski, J.W. Vibrational analysis in gaussian. *help@ gaussian. com* **1999**.
48. Steinberg, G.M.; Swidler, R. The benzohydroxamate anion. *Journal of Organic Chemistry* **1965**, *30*.
49. Arora, R.; Issar, U.; Kakkar, R. Theoretical study of the molecular structure and intramolecular proton transfer in benzohydroxamic acid. *Computational and Theoretical Chemistry* **2017**, *1105*, 18-26.
50. Ochterski, J.W. Thermochemistry in gaussian. *Gaussian Inc* **2000**.
51. Dennington, R.; Keith, T.; Millam, J. Gaussview, version 5. *Semichem Inc., Shawnee Mission, KS* **2009**.
52. Lu, T.; Chen, F. Multiwfn: A multifunctional wavefunction analyzer. *Journal of Computational Chemistry* **2012**, *33*, 580-592.
53. Podlaha, J.; Císařová, I.; Soukupová, L.; Schraml, J. Molecular and crystal structure of benzohydroxamic acid and its ring-substituted derivatives. *Collection of Czechoslovak Chemical Communications* **2000**, *65*, 1273-1288.
54. Marmion, C.J.; Murphy, T.; Starikova, Z.; Nolan, K.B. Redetermination of fac -tris-(benzo-hydrox-am-ato)-iron(iii) tri-hydrate. *Acta Crystallographica* **2000**, *56*, e491–e492.
55. Mikhail Rekharsky; Yoshihisa Inoue, †; Suzanne Tobey; Axel Metzger, A.; Eric Anslyn. Ion-pairing molecular recognition in water: Aggregation at low concentrations that is entropy-driven. *Journal of the American Chemical Society* **2002**, *124*, 14959-14967.
56. Bruneau, E. Quantitative analysis of continuous-variation plots with a comparison of several methods: Spectrophotometric study of organic and inorganic 1:1 stoichiometry complexes. *Journal of Chemical Education* **1992**, *69*, 833.
57. Leon-Pimentel, C.I.; Amaro-Estrada, J.I.; Saint-Martin, H.; Ramirez-Solis, A. Born-oppenheimer molecular dynamics studies of pb(ii) micro hydrated gas phase clusters. *J Chem Phys* **2017**, *146*, 084307.

 doi:10.20944/preprints201806.0110.v1

527 58. Azizi, A.; Ebrahimi, A. The x−···benzohydrazide complexes: The interplay between anion-π and h-bond
528 interactions. *Structural Chemistry* **2016**, *28*, 687-695.
529 59. Lu, T.; Chen, F. Calculation of molecular orbital composition. *Acta Chimica Sinica* **2011**, *69*, 2393-2406.
530 60. Moncomble, A.; Cornard, J.P.; Meyer, M. A quantum chemistry evaluation of the stereochemical activity of the
531 lone pair in pbii complexes with sequestering ligands. *Journal of molecular modeling* **2017**, *23*, 24.

532